

Electronic, Redox, and Photophysical Consequences of Metal-for-Carbon Substitution in Oligo-Phenylene-Ethynylenes

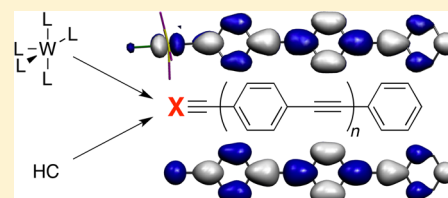
Daniel C. O'Hanlon,[†] Brian W. Cohen,[†] Davis B. Moravec,[†] Richard F. Dallinger,[‡] and Michael D. Hopkins^{*,†}

[†]Department of Chemistry, The University of Chicago, 929 East 57th Street, Chicago, Illinois 60637, United States

[‡]Department of Chemistry, Wabash College, Crawfordsville, Indiana 47933, United States

S Supporting Information

ABSTRACT: The electronic structures, redox chemistry, and excited-state properties of tungsten-containing oligo-phenylene-ethynylenes (OPEs) of the form $W[C(p-C_6H_4CC)_{n-1}Ph](dppe)_2Cl$ ($n = 1-5$; dppe = 1,2-bis-(diphenylphosphino)ethane) are reported and compared with those of organic analogues in order to elucidate the effects of metal-for-carbon substitution on OPE bonding and electronic properties. Key similarities between the metallo- and organic OPEs that bear on materials-related functions include their nearly identical effective conjugation lengths, reduction potentials, and π^* orbital energies and delocalization. In addition to these conserved properties, the tungsten centers endow OPEs with reversible one-electron oxidation chemistry and long-lived emissive triplet excited states that are not accessible to organic OPEs. The electronic similarities and differences between metallo- and organic OPEs can be understood largely on the basis of π/π^* orbital energy matching between tungsten and organic PE fragments and the introduction of an orthogonal mid- π/π^* -gap d orbital in metallo-OPEs. These orbital energies can be tuned by varying the supporting ligands; this provides a means to rationally implement and control the emergent properties of metallo-OPE materials.



centers in metallo-PEs have been incorporated into the backbone between PE segments (A, Chart 1), such as in the

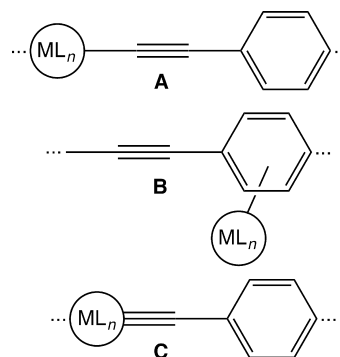
INTRODUCTION

The *p*-phenylene-ethynylene moiety (PE) and its derivatives are primary building blocks of photo- and electro-active π -conjugated molecular assemblies, oligomers, and polymers, because these materials are typically endowed with strong luminescence, controllable electron conductance, structural rigidity, and a myriad of hybrid properties derived therefrom.¹⁻⁵ For example, oligomeric PEs (OPEs) have been widely employed as defined-length bridging units for connecting molecules to each other and to nanostructured or solid surfaces; applications include linkers in donor-bridge-acceptor systems^{6,7} and dye-sensitized solar cells,⁸ chromophore scaffolds for energy transfer and light harvesting,^{7,9} and components for molecular electronics.^{4,10} Along similar lines, polymeric PEs have been developed as sensors,¹¹⁻¹³ organic solar cells,¹⁴ and organic light-emitting diodes^{11,15,16} due to their large exciton mobilities and fluorescence quantum yields.^{11,16} The synthetic parameter space for controlling the electronic structures and properties of organic PE compounds and materials has been extensively explored, with hundreds of derivatives of the parent PE building block having been studied.^{1-5,11,14,15}

In parallel with synthetic-organic approaches to controlling the properties of PE materials, considerable effort has been devoted to developing transition-metal-containing PEs. Interest in these analogues stems from the fact that the metal centers provide complementary avenues for manipulating electronic structure and for introducing properties that are not accessible to all-organic systems.^{2,3,17-19} Most commonly, the metal

centers in metallo-PEs have been incorporated into the backbone between PE segments (A, Chart 1), such as in the

Chart 1. Structural Motifs of Metallo-PEs



extensively studied class of $Pt^{II}L_2$ -containing oligomers and polymers,²⁰ or as pendant groups on the chain (B, Chart 1), as in materials that contain 2,2'-bipyridine units to which are ligated luminescent chromophores (e.g., $Ru^{II}(bpy)_3^{2+}$).^{17,18,21} In contrast to these motifs, in which the metal center is external to the PE building block, in motif C (Chart 1) the PE unit is modified through replacement of an ethynyl carbon atom by a metal center. Because the metal d orbitals are integral to the

Received: November 7, 2013

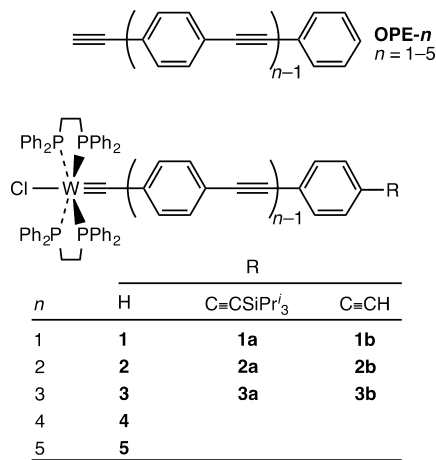
Published: January 31, 2014

$M\equiv C$ bond, the electronic coupling between the metal center and the PE π system in **C** is expected to be stronger than for metallo-PEs of types **A** and **B**, which do not possess substantial metal–ligand multiple-bond character. Thus, these metal–alkylidyne-derived materials afford distinctive opportunities for controlling and enhancing the properties of PE materials.

Among the wide variety of metal–alkylidyne complexes that might be employed as ethynyl-group replacements in type **C** metallo-PEs,²² d^2 $W(\equiv CR)L_4X$ complexes stand out as particularly function-rich building blocks. Characteristic features of these compounds relevant to PE properties include their long-lived phosphorescent excited states,^{23–29} widely tunable oxidation potentials,^{30,31} and stable d^1 metalloradical configurations.^{26,32} Because of these attributes, $W(CR)L_4X$ building blocks have been used to construct a variety of redox- and photoactive metallo-PEs and metallo-ynes that implement their rich properties in electronic and solar-energy-conversion materials.^{23,24,27,28,33–36}

In order to rationally design metallo-PE materials, it is necessary to understand at a fundamental level how the electronic structure–property relationships of organic PEs are affected by the incorporation of metal centers. With this goal in mind, we report a comparative study of the electronic structures and redox and excited-state properties of type **C** tungsten-containing OPEs of the form $W[C(p-C_6H_4CC)_{n-1}Ph](dppe)_2Cl$ (**1–5**, Chart 2; $dppe = 1,2$ -bis(diphenylphosphino)-

Chart 2. Tungsten-Containing and Organic Oligo-Phenylene-Ethynylenes



ethane)³⁷ and of their organic analogues (**OPE-1–OPE-5**, Chart 2). It is found that there are both striking similarities and differences among the electronic structures and properties of these classes of oligomers. Key similarities between metallo- and organic PEs that bear on materials-related functions include their nearly identical effective conjugation lengths, reduction potentials, and π^* orbital energies and delocalization. In addition to these conserved properties, the tungsten centers endow OPEs with reversible one-electron oxidation chemistry and long-lived emissive triplet excited states that are not accessible to organic OPEs. The electronic relationships between these classes of materials can largely be understood on the basis of π/π^* energy matching between tungsten and organic OPE fragments and the introduction in the metallo-PEs of an orthogonal, mid- π/π^* -gap d orbital. The fact that these aspects can be tuned by varying the supporting ligands provides

a means to rationally implement and control the properties derived from the tungsten fragment in metallo-PE materials.

RESULTS AND DISCUSSION

Nature of the Frontier Orbitals. The electronic structures of $W[C(C_6H_4CC)_{n-1}Ph](dppe)_2Cl$ compounds **1–5** and of their organic analogues **OPE-1–OPE-5** (Chart 2) were calculated using density functional theory. The calculated gas-phase molecular structures of **1–5** exhibit nearly identical geometries about their tungsten centers (Table S1 in Supporting Information (SI)) and, like the **OPE-*n*** compounds, essentially planar configurations within their PE units (interphenylene dihedral angles $<4.5^\circ$). Because the key structural features of **1–5** are nearly identical, it may be concluded that the differences among their frontier orbitals and electronic properties are a consequence of the different lengths of their PE alkylidyne ligands.

The frontier orbitals of **1–5** (Figure 1) are derived from the tungsten d_{xz} , d_{yz} , and d_{xy} (t_{2g}) orbitals, as has generally been found for d^2 metal–alkylidyne complexes with compact alkylidyne ligands.^{26,30,38} The HOMOs of all compounds are nearly identical in atomic composition, being principally of tungsten d_{xy} character; this orbital is of π -symmetry with respect to the $dppe$ ligands ($\sim 25\%$ contribution to the HOMO), and nonbonding relative to the axial CPh and Cl ligands (0% contribution; Table S2 in SI). As a consequence of its axial-nonbonding character the HOMO energy is nearly independent of the length of the alkylidyne ligand, spanning a range of only 0.11 eV across the series (Figure 2). The energy and compositional invariance of the d_{xy} -derived HOMO figures prominently in the redox and excited-state properties of **1–5** (vide infra).

The frontier π and π^* orbitals of the PE backbones of **1–5** are the HOMO–1 and LUMO, respectively (Figure 1). These orbitals possess the typical nodal relationships of a corresponding π/π^* orbital pair, such as for the analogous π/π^* orbitals of **OPE-1–OPE-5** (Figure S1, SI), but differ markedly in the extents to which their energies and delocalization depend on the length of the PE chain. The properties of the π^* orbitals of **1–5** are strikingly similar to those of **OPE-1–OPE-5**. In particular, the $\pi^*(WCR)$ and $\pi^*(OPE)$ orbital energies both decrease smoothly with increasing oligomer length, differing by less than 0.3 eV for a given length n (Figure 2). Furthermore, both the $\pi^*(WCR)$ (Figure 1) and $\pi^*(OPE)$ orbitals (Figure S1, SI) are delocalized across the PE chain, with corresponding $[CCC_6H_4]$ subunits of **2–5** and **OPE-2–OPE-5** having very similar amplitudes. The π^* LUMOs of **3** and **OPE-3** (Figure 3) are representative of these close correspondences. For this pair of analogues, the contributions to the π^* orbitals from the terminal $[WC(dppe)_2Cl]$ and $HCCC_6H_4$ units are 30% and 32%, respectively; those from the central $[CCC_6H_4]$ units are 45% and 47%; and the capping CPh units contribute 25% and 22% (Tables S3 and S4, SI). Other pairs of analogues among **1–5** and **OPE-1–OPE-5** exhibit similarly close relationships (Figure S2, SI). Thus, replacement of the $[HCC]$ unit with $[WC(dppe)_2Cl]$ at the terminus of a PE chain results in only a modest perturbation of the energies and delocalization of the OPE π^* LUMOs, despite the strong mixing between the $\pi^*(W\equiv C)$ and $\pi^*[(C_6H_4CC)_{n-1}Ph]$ fragment orbitals.

In contrast to the close relationships between the π^* LUMOs of **1–5** and **OPE-1–OPE-5**, the properties of their π orbitals differ significantly from each other. For **OPE-*n***, the π orbital energy (Figure 2) and delocalization (Figure S1, SI) change

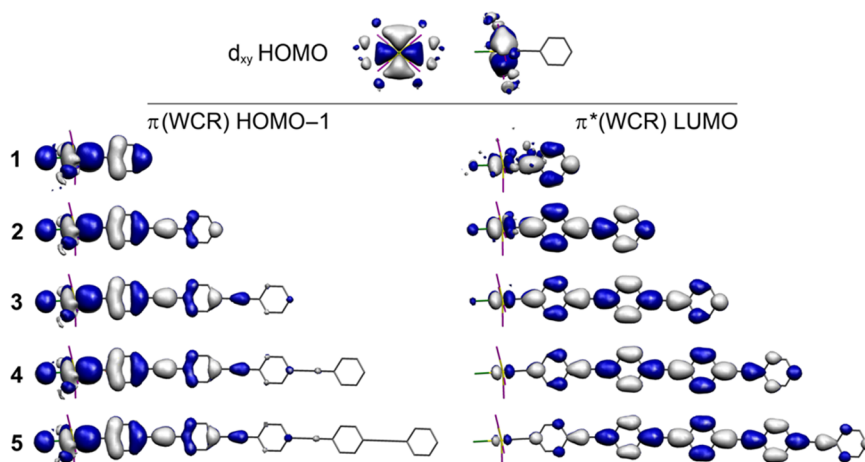


Figure 1. Top: d_{xy} -derived HOMO of **1**, viewed normal to the equatorial and alkyldiyne-ligand planes; the HOMOs of **2–5** are nearly indistinguishable from that of **1**. Bottom: π (WCR) and π^* (WCR) orbitals of **1–5**, viewed normal to the plane of the alkyldiyne ligand. Hydrogen atoms and dppe carbon atoms are omitted for clarity. Orbitals are rendered at iso 0.98 (iso 0.97 for HOMO and LUMO of **1**).

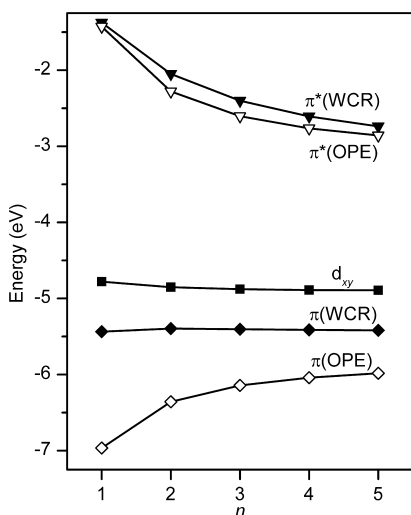


Figure 2. Orbital energies of $W[C(C_6H_4CC)_{n-1}Ph](dppe)_2Cl$ (**1–5**) and $HCC(C_6H_4CC)_{n-1}Ph$ (**OPE-1–OPE-5**).

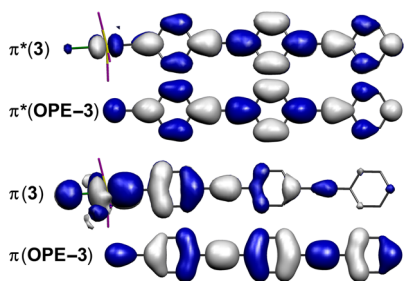


Figure 3. Corresponding π and π^* orbitals of **3** and **OPE-3** (iso 0.98). Hydrogen atoms and dppe carbon atoms are omitted for clarity.

smoothly with increasing chain length in a manner that mirrors the properties of the π^* orbitals described above. The π (WCR) orbitals of **1–5**, in contrast, do not increasingly delocalize as the alkyldiyne ligand is extended (Figure 1). Instead, the principal contribution to these orbitals (>75%) comes from the terminal $[W(CC_6H_4)(dppe)_2Cl]$ unit; for **3–5**, the contributions to π (WCR) from the $[CCC_6H_4]$ units beyond the $[W(CC_6H_4CCC_6H_4)(dppe)_2Cl]$ fragment of **2** total only 4–6% (Table S3, SI). The evident differences in π orbital coefficients

for **3** and **OPE-3** are illustrated in Figure 3; the other pairs of compounds also exhibit large differences (Figure S3, SI). Consistent with their limited delocalization, the energies of the π (WCR) orbitals of **1–5** are independent of the length of the alkyldiyne ligand and span a range of only 0.05 eV; by comparison, the π (OPE) orbital energies of **OPE-1–OPE-5** span a range of 1 eV (Figure 2).

The different behavior of the π (WCR) HOMO–1 and π^* (WCR) LUMO of **1–5** as a function of the length of the PE unit is a consequence of the energy denominators that describe the orbital interactions between the $[W(CC_6H_4)(dppe)_2Cl]$ and $[(CCC_6H_4)_{n-1}H]$ fragments. The close correspondence between the energies and delocalization of the π^* LUMOs of **1–5** and **OPE-1–OPE-5** is traceable to the small difference between the π^* orbital energies of parent compounds **1** and **OPE-1** ($\Delta E(\pi^*) = 0.06$ eV). As a result of the matched π^* energies of the $[HCCC_6H_4]$ and $[W(CC_6H_4)(dppe)_2Cl]$ fragments, their interactions with the π^* orbitals of a given length $[(CCC_6H_4)_{n-1}H]$ fragment are governed by similar energy denominators. In contrast, there is a large difference between the π orbital energies of **1** and **OPE-1** ($\Delta E(\pi) = 1.53$ eV). For the π (WCR) orbitals of extended $W[C(C_6H_4CC)_{n-1}Ph](dppe)_2Cl$ complexes **2–5**, the relatively poor energy match between the π fragment orbitals of the $[W(CC_6H_4)(dppe)_2Cl]$ and $[(CCC_6H_4)_{n-1}H]$ units results in a low degree of mixing compared to that for the π HOMOs of **OPE-*n*** compounds. Although this zero-order energy gap decreases as the chain length increases ($\Delta E(\pi) = 0.56$ eV for **5** and **OPE-5**), fragment-orbital mixing is still limited because the orbitals of longer $[(CCC_6H_4)_{n-1}H]$ fragments are increasingly localized on the central phenylene-ethynylene units rather than near the terminal $[W(CC_6H_4)(dppe)_2Cl]$ fragment. Therefore, the π (WCR) orbitals of **1–5** are primarily of $[W(CC_6H_4)(dppe)_2Cl]$ character and vary little in energy with chain length. The differences between the π (WCR) and π^* (WCR) orbitals of $W[C(C_6H_4CC)_{n-1}Ph](dppe)_2Cl$ complexes are manifested in a number of their electronic properties (vide infra).

Electrochemical Properties. The electrochemistry of $W[C(C_6H_4CC)_{n-1}Ph](dppe)_2Cl$ complexes was investigated to gain insight into how their redox properties differ from those of organic OPEs. Oxidation and reduction potentials for **1–4** are set out in Table 1; cyclic voltammograms are shown in

Table 1. Electrochemical Data for $W[C(C_6H_4CC)_{n-1}Ph](dppe)_2Cl$ Complexes

compd	potential, V vs $FeCp_2^{0/+a}$		
	$E_{1/2}^{0/+}$	$E_{1/2}^{0/-}$	$E_{pc}^{-/n-b}$
1 ^{c,d}	-0.58	-3.39 ^b	
2 ^e	-0.57 ^f	-2.95 ^{b,g}	-3.11, -3.37 ^g
3 ^e	-0.57	-2.54 ^h	-2.86
4 ^e	-0.57	-2.44 ^h	-2.75

^aTHF solution, 25 °C, $\nu = 0.1$ V s⁻¹ unless otherwise indicated. ^bIrreversible, E_{pc} reported. ^cReference 30. ^d0.3 M $[NBu_4][PF_6]$. ^e0.1 M $[NBu_4][PF_6]$. ^f $\nu = 0.5$ V s⁻¹. ^g $\nu = 0.2$ V s⁻¹. ^hQuasi-reversible, $E_{1/2}$ listed.

Figures S4–S6, SI. All compounds exhibit a reversible one-electron oxidation and one or more irreversible reductions. Data for **1** were reported previously as part of a study of the electrochemistry of $d^2 W(CR)L_4X$ complexes in which the CR, L, and X ligands were systematically varied.³⁰ It was found that the first oxidation of these complexes arises from the $(d_{xy})^2/(d_{xy})^1$ couple; because the d_{xy} orbital is axially nonbonding, the oxidation potential is only weakly sensitive to the nature of the CR ligand.³⁰ Consistent with these general observations, and with the invariance of the calculated energy of the d_{xy} -derived HOMO (Figure 2), the oxidation potentials of **1–4** are identical within experimental error ($E_{1/2}^{0/+} = -0.57 \pm 0.01$ V vs $FeCp_2^{0/+}$, Table 1). Organic PEs, which lack the mid- π/π^* -gap d_{xy} redox orbital, are oxidized at much more positive potentials than **1–4**;¹⁶ for example, the onset oxidation potential for polymeric $[C_6H_2(OR)_2CC]_n$ is ~ 0.65 V vs $FeCp_2^{0/+}$.³⁹ Given that the oxidation potentials of simple $W(CR)L_4X$ complexes are tunable over a 2 V range via variation of the electronic properties of the equatorial L ligands,³⁰ it is expected that the potentials of these midgap redox states should be subject to similarly broad synthetic control for other $W[C(C_6H_4CC)_{n-1}Ph]L_4X$ derivatives.

In contrast to the significantly different oxidation properties of metallo- and organic PEs, the reduction properties of these analogues are strikingly similar, with the first reduction potentials of **2–4** (Table 1) being within 0.15 V of those reported for $Ph(CCC_6H_4)_mH$ compounds ($E_p^{0/-}$: **2** = -2.95 V, $PhCCPh$ = -2.95 V; **3** = -2.54 V, $Ph(CCC_6H_4)_2H$ = -2.69 V; **4** = -2.44 V, $Ph(CCC_6H_4)_3H$ = -2.46 V; THF solution, all potentials vs $FeCp_2^{0/+}$).⁴⁰ This observation strongly reinforces the close correlation found between the π^* LUMO energies of **1–5** and **OPE-1–OPE-5** (Figure 2), given that these are the redox orbitals for the process. Indeed, for **1–4** the measured

reduction potentials exhibit an approximate linear correlation with the calculated $\pi^*(WCR)$ LUMO energy (slope = 0.97, RMSD = 0.04 V; Figure S7, SI). In view of the close parallels between the reduction properties of **1–4** and organic PEs, it is predicted that $W[C(C_6H_4CC)_{n-1}Ph](dppe)_2Cl$ derivatives should retain reduction-associated electronic properties of the organic analogues such as their high electron mobilities and low barriers to electron injection in OLEDs,^{2,16} while at the same time providing the new oxidation chemistry noted above.

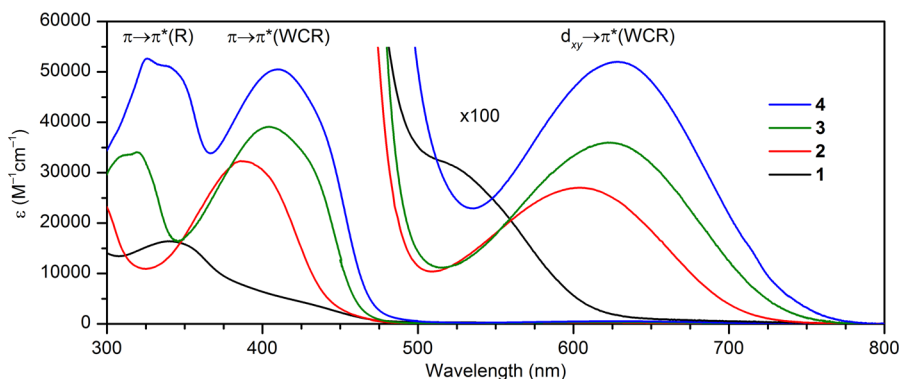
Electronic-Absorption Spectra and Effective Conjugation Length. The electronic-absorption spectra of $W[C(C_6H_4CC)_{n-1}Ph](dppe)_2Cl$ complexes, shown in Figure 4, exhibit bands that are characteristic both of d^2 metal–alkylidyne complexes²⁵ and of organic OPEs. For **1**, the lowest-energy absorption band ($\lambda_{max} = 531$ nm, $\epsilon = 230$ M⁻¹ cm⁻¹; Table 2)

Table 2. Electronic-Absorption Spectroscopic Data for $W[C(C_6H_4CC)_{n-1}Ph](dppe)_2Cl$.^a

compd	λ_{max} nm (ϵ_{max} M ⁻¹ cm ⁻¹)		
	$^1[d_{xy} \rightarrow \pi^*(WCR)]$	$^1[\pi(WCR) \rightarrow \pi^*(WCR)]$	$^1[\pi(R) \rightarrow \pi^*(R)]$
1	531 (230) ^{b,c}	340 (16400) ^b	
2	604 (270) ^d	386 (32300) ^d	
3	623 (360)	404 (39100)	308 (33100), 320 (33800)
4	628 (520)	410 (50500)	326 (52600), 340 (51000)

^aToluene solution, room temperature; spectra in THF solution are similar (Table S5, SI). ^bReference 26. ^cReported as $\lambda_{max} = 525$ nm and $\epsilon_{max} = 310$ M⁻¹ cm⁻¹ in ref 26; values reported here were obtained from deconvolution of the $^1[d_{xy} \rightarrow \pi^*(WCR)]$ band and overlapping bands. ^dReference 27.

has been assigned previously to the spin- and dipole-allowed $^1[d_{xy} \rightarrow \pi^*(WCR)]$ (HOMO→LUMO) transition and the strong band in the near-UV region ($\lambda_{max} = 340$ nm, $\epsilon_{max} = 16400$ M⁻¹ cm⁻¹) has been assigned to the fully allowed $^1[\pi(WCR) \rightarrow \pi^*(WCR)]$ (HOMO-1→LUMO) transition on the basis of TD-DFT calculations.²⁶ Corresponding $^1[d_{xy} \rightarrow \pi^*(WCR)]$ and $^1[\pi(WCR) \rightarrow \pi^*(WCR)]$ absorption bands are observed in the spectra of **2–4** (Figure 4). These bands redshift as the alkylidyne ligand is lengthened, with decreasing marginal shifts from each PE unit. Additionally, the extinction coefficients of the $^1[d_{xy} \rightarrow \pi^*(WCR)]$ and $^1[\pi(WCR) \rightarrow \pi^*(WCR)]$ bands increase by factors of two and three, respectively, between **1** and **4** (Table 2). Qualitatively, this follows the trend observed for the $\pi \rightarrow \pi^*$ transitions of organic analogues of form $Ph(CCC_6H_4)_mH$.^{41,42}

**Figure 4.** Electronic-absorption spectra of $W[C(C_6H_4CC)_{n-1}Ph](dppe)_2Cl$ compounds in toluene.

The shift of the electronic-absorption band maxima for **1–4** as a function of the number of PE units may be used to predict both the optical band gap for a hypothetical infinite-chain-length $W[C(C_6H_4CC)_{n-1}Ph](dppe)_2Cl$ complex and the “effective π conjugation length” of the metal–alkylidyne ligand. It has been observed that the dependence of the $\pi \rightarrow \pi^*$ band energies of conjugated organic oligomers on the number of repeat units is generally well described by the following empirical relationship (eq 1)^{4,43}

$$E_{(n)} = E_{\infty} + (E_1 - E_{\infty})\exp(-a(n - 1)) \quad (1)$$

where $E_{(n)}$ is the band energy for the oligomer of n repeating units, E_1 is the band energy for the monomer, E_{∞} is the band energy for the infinite polymer, and a is an attenuation factor. The fits of the $^1[d_{xy} \rightarrow \pi^*(WCR)]$ and $^1[\pi(WCR) \rightarrow \pi^*(WCR)]$ band energies of **1–4** to eq 1 (Figure 5; see also Figure S8 in

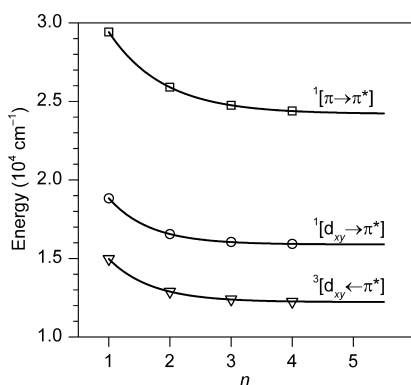


Figure 5. Energies of the $^1[d_{xy} \rightarrow \pi^*(WCR)]$ and $^1[\pi(WCR) \rightarrow \pi^*(WCR)]$ electronic-absorption band maxima and $^3[d_{xy} \rightarrow \pi^*(WCR)]$ emission band maxima of $W[C(C_6H_4CC)_{n-1}Ph](dppe)_2Cl$ compounds. The curves represent the fit of the data to eq 1.

SI) predict that the band maxima for a $W[C(C_6H_4CC)_{n-1}Ph](dppe)_2Cl$ complex with an infinitely long PE alkylidyne ligand lie at $E_{\infty} = 15890 \text{ cm}^{-1}$ (629 nm) for $^1[d_{xy} \rightarrow \pi^*(WCR)]$ and $E_{\infty} = 24200 \text{ cm}^{-1}$ (413 nm) for $^1[\pi(WCR) \rightarrow \pi^*(WCR)]$. These band maxima are red-shifted from those observed for **4** by only 1 nm (30 cm^{-1}) for $^1[d_{xy} \rightarrow \pi^*(WCR)]$ and 3 nm (180 cm^{-1}) for $^1[\pi(WCR) \rightarrow \pi^*(WCR)]$. The effective conjugation length of an oligomer has been defined as that for which the experimentally observed absorption maximum lies within 1 nm of that predicted for the infinite polymer.⁴³ Thus, the behavior of both the $^1[d_{xy} \rightarrow \pi^*(WCR)]$ and $^1[\pi(WCR) \rightarrow \pi^*(WCR)]$ bands of **1–4** indicate that the effective conjugation length of the $W[C(C_6H_4CC)_{n-1}Ph]$ unit is 4–5 repeat units. (The same value is found from an analysis of the emission bands of the compounds, which are described below.)⁴⁴ This conjugation length is the same as that found for organic PE analogues of the form $p\text{-Et}_2\text{N}_3(3\text{-R-C}_6\text{H}_3\text{CC})_n\text{SiMe}_3$ ($R = \text{alkyl}$, $n \leq 16$), for which a fit of $\pi \rightarrow \pi^*$ absorption-band energies to eq 1 provides a conjugation length of 5 repeat units.⁴³

The electronic-absorption spectra of **3** and **4** also exhibit strong bands in the 300–350 nm region whose properties are consistent with assignment to alkylidyne-ligand-localized $^1[\pi(R) \rightarrow \pi^*(R)]$ transitions (Figure 4 and Table 2). Unlike the featureless $^1[d_{xy} \rightarrow \pi^*(WCR)]$ and $^1[\pi(WCR) \rightarrow \pi^*(WCR)]$ bands, these ligand-centered bands exhibit vibronic shoulders whose spacing ($\sim 1200\text{--}1300 \text{ cm}^{-1}$) is consistent with assignment to phenylene-based stretching modes.⁴⁵ The

positions and shapes of these bands overlay closely with those of the lowest-energy $^1[\pi \rightarrow \pi^*]$ bands of analogous organic OPEs ($\lambda_{\text{max}}(\mathbf{3}) = 320 \text{ nm}$, $\lambda_{\text{max}}(\text{Ph}(\text{CCC}_6\text{H}_4)_2\text{H}) = 320 \text{ nm}$; $\lambda_{\text{max}}(\mathbf{4}) = 326 \text{ nm}$, $\lambda_{\text{max}}(\text{Ph}(\text{CCC}_6\text{H}_4)_3\text{H}) = 340 \text{ nm}$; Figures S9–S10 in SI),⁴² suggesting that the orbitals between which these transitions occur have small contributions from the $[W(C)(dppe)_2Cl]$ unit. For hypothetical $W[C(C_6H_4CC)_{n-1}Ph](dppe)_2Cl$ compounds with PE alkylidyne ligands longer than that of **4**, it is expected that these ligand-localized $^1[\pi(R) \rightarrow \pi^*(R)]$ bands will continue to lie to higher energy of the $^1[\pi(WCR) \rightarrow \pi^*(WCR)]$ and $^1[d_{xy} \rightarrow \pi^*(WCR)]$ bands, based on their predicted positions for hypothetical infinite-length compounds ($\lambda_{\text{max}}(n = \infty)$: $^1[\pi(R) \rightarrow \pi^*(R)]$, $\sim 375 \text{ nm}$;^{43,46} $^1[\pi(WCR) \rightarrow \pi^*(WCR)]$, 413 nm; $^1[d_{xy} \rightarrow \pi^*(WCR)]$, 629 nm).

Excited-State Properties. In contrast to the high-quantum-yield $^1[\pi\pi^*]$ fluorescence observed for organic PE oligomers and polymers,^{2,15} the $W[C(C_6H_4CC)_{n-1}Ph](dppe)_2Cl$ complexes phosphoresce in fluid solution at room temperature (Figure 6 and Table 3). The emission from **1** has

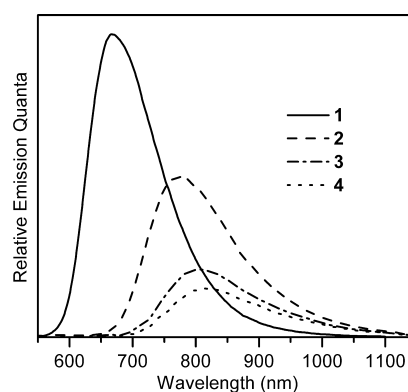


Figure 6. Emission spectra of $W[C(C_6H_4CC)_{n-1}Ph](dppe)_2Cl$ compounds in toluene at room temperature. Band areas reflect the emission quantum yields.

been previously assigned as originating from the $^3[(d_{xy})^1(\pi^*(WCPH))]^1$ excited state, based on electronic-structure calculations and the fact that the excited-state structure determined by X-ray transient-absorption measurements is consistent with that anticipated for the $(d_{xy})^1(\pi^*(WCPH))^1$ configuration.²⁶ The emission bands of **1–4** redshift with lengthening of the OPE ligand and maintain nearly constant band widths and Stokes shifts relative to the $^1[d_{xy} \rightarrow \pi^*(WCR)]$ absorption band (Table 3); this both supports assignment of the emissive state as $^3[(d_{xy})^1(\pi^*(WCR))]^1$ for all compounds in the series and is consistent with an effective conjugation length of 4–5 units (Figure 5).⁴⁴ In view of the prediction from the preceding section that the $^1[(d_{xy})^1(\pi^*(WCR))]^1$ state will lie lower in energy than the PE-ligand-localized $^1[\pi\pi^*]$ state at the limit of an infinitely long alkylidyne ligand, it is anticipated that $W[C(C_6H_4CC)_{n-1}Ph](dppe)_2Cl$ derivatives with longer ligands will not exhibit PE-like $^1[\pi\pi^*]$ fluorescence unless the emitting segment can be spatially decoupled from the metal-derived excited states.

The luminescence lifetimes and quantum yields of compounds **1–4** depend strongly on the length of the PE unit, with the lifetimes (τ_{em}) decreasing from 303 to 39 ns and the quantum yield (ϕ_{em}) from 0.017 to 0.0025 from **1** to **4** (Table 3). These differences are the result of an 8-fold increase

Table 3. Emission Spectroscopic and Photophysical Data for the $^3[(d_{xy})^1(\pi^*(WCR))^1]$ State of $W[C(C_6H_4CC)_{n-1}Ph](dppe)_2Cl$ Complexes.^a

compd	λ_{max} , nm	Stokes shift, cm^{-1b}	fwhm, cm^{-1}	τ_{em} , ns	ϕ_{em}	k_r^c , $10^4 s^{-1}$	k_{nr}^d , $10^6 s^{-1}$
1	668 ^e	3860	2760	303 ^e	0.017 ^e	5.61	3.24
2	776 ^f	3670	2640	106 ^f	0.0081 ^{f,g}	7.64	9.36
3	806	3640	2540	49	0.0035	7.14	20.3
4	816	3670	2520	39	0.0025	6.41	25.6

^aToluene solution, room temperature. ^bShift from the $^1[d_{xy} \rightarrow \pi^*(WCR)]$ absorption band (Table 3). ^c $k_r = \phi_{em}/\tau_{em}$. ^d $k_{nr} = 1/\tau_{em} - k_r$. ^eReference 26. ^fReference 27. ^gThe quantum yield reported here is larger than that reported in ref 27 by a factor of 1.5; this scaling reflects the subsequent revision to the absolute quantum yield of the $Ru(bpy)_3^{2+}$ reference compound from $\phi = 0.042$ to 0.063 (ref 47).

in the nonradiative decay rate (k_{nr}) across the series; the radiative rate remains constant. This contrasts with the behavior of organic OPEs, for which the fluorescence lifetime decreases with oligomer length due to an increase in the radiative rate.⁴⁸ For 2–4, the differences in nonradiative rate appear to be a manifestation of decay in the weak-coupling limit, as indicated by the observation of a linear (energy-gap-law) correlation between $\ln(k_{nr})$ and E_{em} (Figure 7).⁴⁹ Because

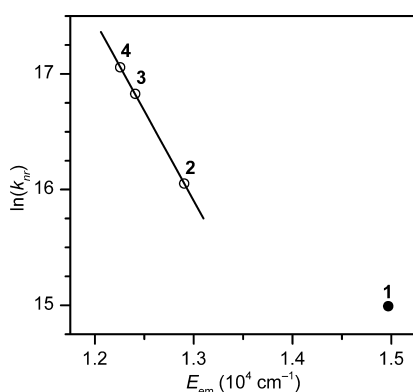


Figure 7. Energy-gap law plot for the emissive $^3[(d_{xy})^1(\pi^*(WCR))^1]$ excited states of 1–4. The line is a linear fit to the data for 2–4: $\ln(k_{nr}) = -0.00155E_{em} + 36.108$ ($R^2 = 0.9999$).

the energy of the $^3[(d_{xy})^1(\pi^*(WCR))^1]$ excited-state energy of 4 approaches that predicted for a hypothetical complex with an infinite-length OPE ligand (Figure 5),⁴⁴ the conformation of these compounds to the energy-gap law suggests that chromophores with longer OPE ligands will possess emission lifetimes of magnitude comparable to that of 4 (in the absence of new nonradiative decay modes introduced by the extended ligands). The nonradiative rate of 1 deviates significantly from the linear correlation for 2–4 ($k_{nr}(\text{obs}) = 3.24 \times 10^6 s^{-1}$, $k_{nr}(\text{pred}) = 3.36 \times 10^5 s^{-1}$), indicating the presence of an additional nonradiative decay pathway. Comparison of the temperature dependence of the nonradiative decay rates of 1 and 2 shows that at room temperature 1 additionally decays via thermal population of a higher-lying excited state (see Figure S11, Tables S6 and S7, and associated discussion in the SI). That the energy gap between the emissive $^3[(d_{xy})^1(\pi^*(WCR))^1]$ excited state and next higher-lying excited state is considerably smaller for 1 than for 2–4 is indicated by their electronic-absorption spectra (Figure 4), which show that for 1 the $^1[d_{xy} \rightarrow \pi^*(WCR)]$ band strongly overlaps with the higher-lying absorption band whereas for 2–4 these bands are well separated. Based on an Arrhenius analysis of emission lifetime data (see the SI), the room-temperature nonradiative rate of 1 would lie in the range $\sim 5.7\text{--}7.8 \times 10^5 s^{-1}$ in the absence of the

thermally activated nonradiative decay channel; this is in reasonable agreement with that predicted by extrapolation of the energy-gap-law fit to the rates of 2–4 ($3.36 \times 10^5 s^{-1}$), given the uncertainties inherent in extrapolating the two relationships. We conclude, therefore, that 1 would conform to the broader energy-gap-law relationship exhibited by 2–4 if the higher-activation-energy nonradiative decay channel were not present.

To further probe the properties of the emissive excited-states of $W[C(C_6H_4CC)_{n-1}Ph](dppe)_2Cl$ complexes, the transient-absorption spectra of 1–4 were measured. The spectra acquired $\sim 7\text{--}10$ ps following excitation are shown in Figure 8. These

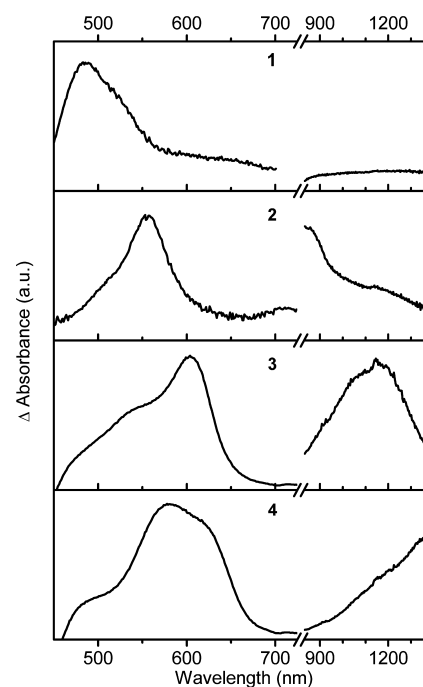


Figure 8. Transient-absorption spectra of 1–4 in toluene ($\lambda_{ex} = 400$ nm) at $\Delta t \cong 5(\tau_{rise})$. Values of ΔA in the 440–760 nm and 850–1400 nm regions are not comparable because the spectra are acquired on separate instruments at different laser powers.

time points are those at which the prominent features in the spectra have reached their maximum absorbance, and following which the spectra decay according to the emission lifetime but do not evolve in shape; thus, they originate from the thermally equilibrated $^3[(d_{xy})^1(\pi^*(WCR))^1]$ excited state of each compound. Kinetic analyses of time-resolved spectra provide time constants for the rise of the features shown in Figure 8 of $\tau_{rise} \cong 1\text{--}2$ ps (Figures S12–S14, SI), which presumably reflects vibrational cooling and/or intersystem crossing from a higher-lying singlet state to the emissive $^3[(d_{xy})^1(\pi^*(WCR))^1]$

Table 4. Ground-State and $^3[(d_{xy})^1(\pi^*(WCR))^1]$ Excited-State Electronic-Absorption Bands of $W[C(C_6H_4CC)_{n-1}Ph](dppe)_2Cl$ Complexes

cmpd	λ_{max} nm			
	$^1[\pi(WCR) \rightarrow \pi^*(WCR)]^a$	$^3[\pi(WCR) \rightarrow \pi^*(WCR)]_{TA}$	$^3[\pi^*(WCR) \rightarrow \pi^*_n]_{TA}$	$\Delta E, \text{cm}^{-1b}$
1	340	420		7440
2	386	555	800–900	7890
3	404	604, 540 (sh)	1130	8200
4	410	620 (sh), 580, 485 (sh)	1370	8260

^aTable 2. ^b $\Delta E = E(^1[\pi(WCR) \rightarrow \pi^*(WCR)]) - E(^3[\pi(WCR) \rightarrow \pi^*(WCR)]_{TA})$, measured at the lowest-energy shoulder.

state. The spectra of **1–4** each exhibit a prominent band in the visible region, and **2–4** also show a strong, broad band in the near-infrared region; the positions of these bands are set out in Table 4. The spectra of **3** and **4** exhibit the bleaching of the ground state $^1[\pi(WCR) \rightarrow \pi^*(WCR)]$ absorbance near 450 nm, while for **1** and **2** the equivalent features lie outside the wavelength range of the experiment. Bleaching of the $^1[d_{xy} \rightarrow \pi^*(WCR)]$ absorption band is not observed for any of the compounds due to its relatively small extinction coefficient ($\epsilon \leq 520 \text{ M}^{-1} \text{ cm}^{-1}$, Table 2).

The transient absorption bands of **1–4** in the visible region are assigned to the spin- and dipole-allowed transition $^3[(\pi(WCR))^2(d_{xy})^1(\pi^*(WCR))^1 \rightarrow (\pi(WCR))^1(d_{xy})^1(\pi^*(WCR))^2]$ (denoted $^3[\pi(WCR) \rightarrow \pi^*(WCR)]_{TA}$ in Table 4), based on their similarity to the ground-state $^1[\pi(WCR) \rightarrow \pi^*(WCR)]$ absorption bands. For **1**, **1b**, and **2**, it was possible to derive the excited-state electronic-absorption spectra in the visible region from nanosecond-time-scale transient-absorption spectra (Figure 9).⁵⁰ The close correspondence in shape and extinction

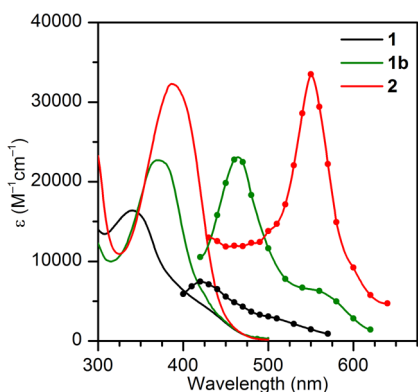


Figure 9. Electronic-absorption spectra of the ground states (solid line) and $^3[(d_{xy})^1(\pi^*(WCR))^1]$ excited states (data indicated by solid circles, connected by a smooth curve) of **1**, **1b**, and **2** in toluene.

coefficient between the ground-state and excited-state $\pi \rightarrow \pi^*$ bands of these compounds is evident. Further, the ground and excited-state $\pi \rightarrow \pi^*$ bands of **1–4** exhibit parallel shifts in energy as a function of the length of the OPE ligand ($\Delta E = 7440\text{--}8200 \text{ cm}^{-1}$, Table 4); this suggests that the effective conjugation length within the tungsten-PE unit in the $^3[(d_{xy})^1(\pi^*(WCR))^1]$ excited state is 4–5 repeat units, which is the same as that found for the ground state (vide supra). The intense bands observed in the near-infrared region for **2–4** (Figure 8) are assigned to spin- and dipole-allowed transitions between orbitals within the π^* manifold, specifically, $^3[(d_{xy})^1(\pi^*(WCR))^1(\pi^*_n)^0 \rightarrow (d_{xy})^1(\pi^*(WCR))^0(\pi^*_n)^1]$ (denoted $^3[\pi^*(WCR) \rightarrow \pi^*_n]_{TA}$), where π^*_n is a LUMO+ n WCR or OPE-localized orbital. The transition energies of the near-

infrared band are more strongly dependent on the length of the PE unit than are the $^3[\pi(WCR) \rightarrow \pi^*(WCR)]_{TA}$ bands; the $^3[\pi(WCR) \rightarrow \pi^*(WCR)]_{TA}$ band red shifts only 430 cm^{-1} between **3** and **4**, whereas $^3[\pi^*(WCR) \rightarrow \pi^*_n]_{TA}$ red shifts 1550 cm^{-1} . The larger marginal red shift is likely due to the increased density of orbitals in the π^* manifold as the tungsten-PE unit increases in length.

An important difference between the transient-absorption spectra of $W[C(C_6H_4CC)_{n-1}Ph](dppe)_2Cl$ complexes and those of organic analogues is in their temporal evolution. The transient-absorption spectrum of the $S_1 \pi \rightarrow \pi^*$ state of $Ph(CCC_6H_4)_2H$ (an analogue of **3**) exhibits features that appear within 3 ps and then red-shift over the next 50 ps.⁵¹ Corresponding evolution on these time scales of the transient-absorption and fluorescence spectra of longer organic OPEs has also been observed.^{48,52} In contrast to these observations, the transient-absorption bands of **1–4** do not shift in position or change shape over the course of their decay. The longer-time spectral evolution of the organic OPEs has been interpreted as arising from planarization of the PE units in the excited state.^{48,51,52} In the ground state in solution at room temperature, OPEs possess a broad distribution of torsional angles due to the small barrier to rotation (0.5 kcal/mol);⁵³ this barrier is larger in $^1[\pi\pi^*]$ excited states due to increased quinoidal/cumulenenic character associated with the excited-state structural distortions.

The logical inference from these observations is that the tungsten-PE units of extended derivatives **2–4** do not (fully) planarize in the $^3[(d_{xy})^1(\pi^*(WCR))^1]$ excited state, and that their excited-state torsional barriers are smaller than for their organic analogues. This can be understood on the basis of the different orbital configurations of the $^3[(d_{xy})^1(\pi^*(WCR))^1]$ and $^1[\pi\pi^*]$ excited states. Although both states are characterized by singly occupied π^* orbitals, the depopulated orbital for the organic compounds is π bonding and for **1–4** is the axially nonbonding d_{xy} orbital. Thus, for an oligomer of given length, the changes in formal π bond order associated with planarizing quinoidal/cumulenenic distortions are smaller for the $^3[(d_{xy})^1(\pi^*(WCR))^1]$ state than for the $^1[\pi\pi^*]$ state. Relevant to this point, a recent study of the structure of **1** in the $^3[(d_{xy})^1(\pi^*(WCR))^1]$ state using X-ray transient-absorption spectroscopy and DFT calculations²⁶ found that, relative to the ground state, the $WC-C_{ipso}$ bond contracts by 0.041 \AA (a cumulenenic distortion) and the phenyl group undergoes a quinoidal distortion characterized by the displacement parameter $\delta r = 0.038 \text{ \AA}$.⁵⁴ By comparison, the distortions of the analogous $S_2 \ ^1[\pi\pi^*]$ state of OPE-1 are roughly twice as large ($\Delta d(HC-C_{ipso}) = 0.071 \text{ \AA}$, $\delta r = 0.072 \text{ \AA}$), consistent with the 2-fold larger change in formal bond orders.⁵⁵ These observations support the hypothesis that the lack of longer-time evolution of the transient-absorption spectra of **2–4** manifests a

small perturbation to their ground-state torsional distributions, due to a small increase in excited-state torsional barriers relative to their organic analogues.

CONCLUSIONS

The substitution of a tungsten center for the terminal ethynyl carbon atom in an oligo-phenylene-ethynylene, yielding the $W[C(C_6H_4CC)_{n-1}Ph](dppe)_2Cl$ family of compounds (**1–5**), preserves the molecular structure and key electronic properties of the organic materials and provides a locus for introducing new functionality. The metallo- and organic OPEs are found to possess similar effective π -conjugation lengths (4–5 PE units), first reduction potentials, π^* orbital energies and amplitudes, and OPE-centered $\pi \rightarrow \pi^*$ electronic-absorption bands. In addition to these conserved properties, the metallo-OPEs also undergo reversible one-electron oxidation at potentials approximately 1 V lower than those of organic OPEs, and long-lived phosphorescence from the $^3[(d_{xy})^1(\pi^*(WCR))^1]$ state instead of the $^1[\pi\pi^*]$ fluorescence characteristic of organic OPEs. The different excited-state orbital configurations of organic ($^1[\pi\pi^*]$) and metallo ($^3[(d_{xy})^1(\pi^*(WCR))^1]$) OPEs affect the excited-state barrier to rotation in the PE backbone and, in a point that remains under investigation, may be important for the contrasting PE-length dependences of their radiative rates (which are sizable for organic OPEs and negligible for **1–4**) and nonradiative rates (small for organic OPEs, sizable for **1–4**).

The fact that the conserved and new properties of metallo-OPEs **1–4** can be understood largely on the basis of the π , π^* , and d_{xy} orbital energies, which for tungsten-alkylidyne complexes are known to be sensitive to the nature of the supporting ligands, suggests that it should be possible to control these properties through compositional variation. It has previously been shown for $W(CR)L_4X$ compounds that the oxidation potential is linearly correlated with the calculated d_{xy} orbital energy, and can be tuned over a 2 V range by varying the equatorial ligands.³⁰ The oxidation potentials of **1–4** conform to this correlation; thus, these empirical relationships should be directly applicable to the design of new redox-active metallo-OPEs with other ligand sets. Similarly, variation of the supporting ligands of $W(CR)L_4X$ compounds can strongly affect $\pi(WCR)$ and $\pi^*(WCR)$ orbital energies; this provides a means to modulate the interactions among the fragment π/π^* orbitals of the $[W(CC_6H_4)L_4X]$ and $[(CCC_6H_4)_{n-1}H]$ subunits. For example, in the series of compounds $W(CPh)(dppe)_2Cl$ (**1**), $W(CPh)(dppe)(CO)_2Cl$, and $W(CPh)(CO)_4Cl$, the $\pi(WCPh)$ and $\pi^*(WCPh)$ orbital energies are calculated to decrease by 0.6–0.8 eV with each substitution of a dppe ligand by two CO ligands.³⁰ The close correspondences among the π^* orbitals (and associated properties) of **1–5** and OPE-1–OPE-5 are due to the nearly identical π^* fragment-orbital energies of the $[W(CC_6H_4)(dppe)_2Cl]$ and $[(CCC_6H_4)_{n-1}H]$ subunits, and the dissimilarities between the π orbitals of **1–5** and OPE-1–OPE-5 arise from the ~ 1.5 eV mismatch between the corresponding π fragment orbitals. Thus, incorporating a $[W(CO)_4Cl]$ subunit into an OPE should bring the $\pi(WCR)$ and $\pi(OPE)$ fragment orbitals into resonance and decouple the $\pi^*(WCR)$ and $\pi^*(OPE)$ fragment orbitals, while the mixed-ligand $[W(dppe)(CO)_2Cl]$ unit would provide intermediate mixing of the π and π^* levels. The ability to tune the delocalization of both the π and π^* orbitals could have applications for redox- and photoactive materials, such as in selectively promoting or disfavoring hole or electron transfer.

Work is underway to test these predictions in new metallo-OPE derivatives of type C.

ASSOCIATED CONTENT

Supporting Information

Synthetic procedures and characterization data for **2a**, **2b**, **3**, **3a**, **3b**, **4**, and selected starting materials; experimental procedures for electronic absorption and emission spectra, emission lifetimes and quantum yields, transient-absorption spectra, cyclic voltammograms, and density functional calculations; tables of bond distances, Cartesian coordinates, orbital energies, and orbital atomic parentages provided by density functional theory calculations; tables of electronic-absorption band maxima, temperature-dependent emission lifetime data, and Arrhenius fitting parameters for emission lifetimes; figures showing electrochemical data, electronic spectroscopic data, kinetic analyses of transient-absorption spectra, and calculated frontier orbitals. This material is available free of charge via the Internet at <http://pubs.acs.org>.

AUTHOR INFORMATION

Corresponding Author

mhopkins@uchicago.edu

Notes

The authors declare no competing financial interest.

ACKNOWLEDGMENTS

This research was supported by the U.S. Department of Energy, Office of Basic Energy Sciences, Solar Photochemistry Program, under Grant DE-FG02-07-ER15910. Use of the Center for Nanoscale Materials (CNM) was supported by the U.S. Department of Energy, Office of Science, Office of Basic Energy Sciences, under Contract No. DE-AC02-06CH11357. Mass spectrometry facilities were supported in part by National Science Foundation Grant CHE-1048528. We are grateful to Dr. Gary P. Wiederrecht and Dr. David J. Gosztola of the Center for Nanoscale Materials at Argonne National Laboratory for their assistance with the picosecond transient-absorption measurements, and Dr. Shuijiang Yang for assistance with some of the DFT calculations.

REFERENCES

- (1) *Poly(arylene ethynylene)s: From Synthesis to Application*; Weder, C., Ed.; Springer-Verlag: Berlin, 2005.
- (2) Bunz, U. H. F. *Chem. Rev.* **2000**, *100*, 1605.
- (3) Schwab, P. F. H.; Levin, M. D.; Michl, J. *Chem. Rev.* **1999**, *99*, 1863.
- (4) Martin, R. E.; Diederich, F. *Angew. Chem., Int. Ed.* **1999**, *38*, 1350.
- (5) Giesa, R. *Macromol. Sci. Rev. Chem. Phys.* **1996**, *C36*, 631.
- (6) (a) Wenger, O. S. *Acc. Chem. Res.* **2011**, *44*, 25. (b) Odobel, F.; Fortage, J. C. R. *Chem.* **2009**, *12*, 437. (c) Albinsson, B.; Mårtensson, J. *Photochem. Photobiol., C* **2008**, *9*, 138.
- (7) Holten, D.; Bocian, D. F.; Lindsey, J. S. *Acc. Chem. Res.* **2001**, *35*, 57.
- (8) (a) Johansson, P. G.; Kopecky, A.; Galoppini, E.; Meyer, G. J. *J. Am. Chem. Soc.* **2013**, *135*, 8331. (b) Stalder, R.; Xie, D.; Zhou, R.; Xue, J.; Reynolds, J. R.; Schanze, K. S. *Chem. Mater.* **2012**, *24*, 3143. (c) Jiang, H.; Taranekekar, P.; Reynolds, J. R.; Schanze, K. S. *Angew. Chem., Int. Ed.* **2009**, *48*, 4300. (d) Myahkostupov, M.; Piotrowiak, P.; Wang, D.; Galoppini, E. *J. Phys. Chem. C* **2007**, *111*, 2827. (e) Taratula, O.; Rochford, J.; Piotrowiak, P.; Galoppini, E.; Carlisle, R. A.; Meyer, G. J. *J. Phys. Chem. B* **2006**, *110*, 15734. (f) Wang, D.; Mendelsohn, R.; Galoppini, E.; Hoertz, P. G.; Carlisle, R. A.; Meyer, G. J. *J. Phys. Chem. B* **2004**, *108*, 16642.

- (9) (a) Yin, S.; Leen, V.; Jackers, C.; Beljonne, D.; Van Averbeke, B.; Van der Auweraer, M.; Boens, N.; Dehaen, W. *Chem.—Eur. J.* **2011**, *17*, 13247. (b) Harriman, A.; Mallon, L. J.; Elliot, K. J.; Haefele, A.; Ulrich, G.; Ziesel, R. *J. Am. Chem. Soc.* **2009**, *131*, 13375. (c) Atienza, C.; Insuasty, B.; Seoane, C.; Martin, N.; Ramey, J.; Rahman, G. M. A.; Guldi, D. M. *J. Mater. Chem.* **2005**, *15*, 124. (d) Zhao, Y.; Shirai, Y.; Slepko, A. D.; Cheng, L.; Alemany, L. B.; Sasaki, T.; Hegmann, F. A.; Tour, J. M. *Chem.—Eur. J.* **2005**, *11*, 3643.
- (10) (a) Kaur, I.; Zhao, X.; Bryce, M. R.; Schauer, P. A.; Low, P. J.; Katakly, R. *ChemPhysChem* **2013**, *14*, 431. (b) Moore, A. M.; Mantooth, B. A.; Dameron, A. A.; Donhauser, Z. J.; Lewis, P. A.; Smith, R. K.; Fuchs, D. J.; Weiss, P. S. In *Frontiers in Materials Research*; Fujikawa, Y., Nakajima, K., Sakurai, T., Eds.; Springer-Verlag: Berlin, 2008, p 29. (c) Newton, M. D.; Smalley, J. F. *Phys. Chem. Chem. Phys.* **2007**, *9*, 555. (d) Dube, A.; Chadeayne, A. R.; Sharma, M.; Wolczanski, P. T.; Engstrom, J. R. *J. Am. Chem. Soc.* **2005**, *127*, 14299. (e) James, D. K.; Tour, J. M. *Top. Curr. Chem.* **2005**, *257*, 33. (f) Mantooth, B. A.; Weiss, P. S. *Proc. IEEE* **2003**, *91*, 1785. (g) Tour, J. M. *Acc. Chem. Res.* **2000**, *33*, 791. (h) Dhirani, A.; Lin, P.-H.; Guyot-Sionnest, P.; Zehner, R. W.; Sita, L. R. *J. Chem. Phys.* **1997**, *106*, 5249.
- (11) Andrew, T. L.; Swager, T. M. *J. Polym. Sci., Part B: Polym. Phys.* **2011**, *49*, 476.
- (12) Thomas, S. W.; Joly, G. D.; Swager, T. M. *Chem. Rev.* **2007**, *107*, 1339.
- (13) Swager, T. M.; Zheng, J. In *Poly(arylene ethynylene)s: From Synthesis to Application*; Weder, C., Ed.; Springer-Verlag: Berlin, 2005, p 151.
- (14) Cheng, Y.-J.; Yang, S.-H.; Hsu, C.-S. *Chem. Rev.* **2009**, *109*, 5868.
- (15) Grimsdale, A. C.; Leok Chan, K.; Martin, R. E.; Jokisz, P. G.; Holmes, A. B. *Chem. Rev.* **2009**, *109*, 897.
- (16) Voskerician, G.; Weder, C. In *Poly(arylene ethynylene)s: From Synthesis to Application*; Weder, C., Ed.; Springer-Verlag: Berlin, 2005, p 209.
- (17) Liu, Y.; Li, Y.; Schanze, K. S. *J. Photochem. Photobiol., C* **2002**, *3*, 1.
- (18) Ley, K. D.; Schanze, K. S. *Coord. Chem. Rev.* **1998**, *171*, 287.
- (19) (a) Low, P. J. *Coord. Chem. Rev.* **2013**, *257*, 1507. (b) Whittell, G. R.; Hager, M. D.; Schubert, U. S.; Manners, I. *Nat. Mater.* **2011**, *10*, 176. (c) Eloi, J.-C.; Chabanne, L.; Whittell, G. R.; Manners, I. *Mater. Today* **2008**, *11*, 28. (d) Williams, K. A.; Boydston, A. J.; Bielawski, C. W. *Chem. Soc. Rev.* **2007**, *36*, 729. (e) Klemm, E.; Pautzsch, T.; Blankenburg, L. In *Poly(arylene ethynylene)s: From Synthesis to Application*; Weder, C., Ed.; Springer-Verlag: Berlin, 2005, p 53. (f) Kingsborough, R. P.; Swager, T. M. *Prog. Inorg. Chem.* **1999**, *48*, 123.
- (20) (a) Liao, C.; Shelton, A. H.; Kim, K.-Y.; Schanze, K. S. *ACS Appl. Mater. Interfaces* **2011**, *3*, 3225. (b) Muro, M. L.; Rachford, A. A.; Wang, X.; Castellano, F. N. *Top. Organomet. Chem.* **2010**, *29*, 1. (c) Silverman, E. E.; Cardolaccia, T.; Zhao, X.; Kim, K.-Y.; Haskins-Glusac, K.; Schanze, K. S. *Coord. Chem. Rev.* **2005**, *249*, 1491.
- (21) (a) Kokil, A.; Yao, P.; Weder, C. *Macromolecules* **2005**, *38*, 3800. (b) Walters, K. A.; Ley, K. D.; Cavalaheiro, C. S. P.; Miller, S. E.; Gosztola, D.; Wasielewski, M. R.; Bussandri, A. P.; van Willigen, H.; Schanze, K. S. *J. Am. Chem. Soc.* **2001**, *123*, 8329. (c) Ley, K. D.; Li, Y.; Johnson, J. V.; Powell, D. H.; Schanze, K. S. *Chem. Commun.* **1999**, 1749.
- (22) (a) Shi, C. A.; Jia, G. C. *Coord. Chem. Rev.* **2013**, *257*, 666. (b) Herndon, J. W. *Coord. Chem. Rev.* **2012**, *256*, 1281. (c) Míndiola, D. J.; Bailey, B. C.; Basuli, F. *Eur. J. Inorg. Chem.* **2006**, *2006*, 3135. (d) Schrock, R. R. *Chem. Rev.* **2002**, *102*, 145. (e) Fischer, H.; Hofmann, P.; Kreissl, F. R.; Schrock, R. R.; Schubert, U.; Weiss, K. *Carbyne Complexes*; VCH Publishers: Weinheim, Germany, 1988.
- (23) Mayr, A.; Yu, M. P. Y.; Yam, V. W.-W. *J. Am. Chem. Soc.* **1999**, *121*, 1760.
- (24) Yu, M. P. Y.; Yam, V. W.-W.; Cheung, K.-K.; Mayr, A. *J. Organomet. Chem.* **2006**, *691*, 4514.
- (25) Da Re, R. E.; Hopkins, M. D. *Coord. Chem. Rev.* **2005**, *249*, 1396.
- (26) Lovaasen, B. M.; Lockard, J. V.; Cohen, B. W.; Yang, S.; Zhang, X.; Simpson, C. K.; Chen, L. X.; Hopkins, M. D. *Inorg. Chem.* **2012**, *51*, 5660.
- (27) Cohen, B. W.; Lovaasen, B. M.; Simpson, C. K.; Cummings, S. D.; Dallinger, R. F.; Hopkins, M. D. *Inorg. Chem.* **2010**, *49*, 5777.
- (28) Moravec, D. B.; Hopkins, M. D. *J. Phys. Chem. A* **2013**, *117*, 1744.
- (29) (a) Jelliss, P. A.; Wampler, K. M. *Organometallics* **2005**, *24*, 707. (b) Lee, F.-W.; Chan, M. C.-W.; Cheung, K.-K.; Che, C.-M. *J. Organomet. Chem.* **1998**, *552*, 255. (c) Lee, F.-W.; Chi-Wang Chan, M.; Cheung, K.-K.; Che, C.-M. *J. Organomet. Chem.* **1998**, *563*, 191. (d) Bocarsly, A. B.; Cameron, R. E.; Mayr, A.; McDermott, G. A. In *Photochemistry and Photophysics of Coordination Compounds*; Yersin, H., Vogler, A., Eds.; Springer-Verlag: Berlin, 1987, p 213. (e) Bocarsly, A. B.; Cameron, R. E.; Rubin, H. D.; McDermott, G. A.; Wolff, C. R.; Mayr, A. *Inorg. Chem.* **1985**, *24*, 3976.
- (30) Haines, D. E.; O'Hanlon, D. C.; Manna, J.; Jones, M. K.; Shaner, S. E.; Sun, J.; Hopkins, M. D. *Inorg. Chem.* **2013**, *52*, 9650.
- (31) (a) Pombeiro, A. J. L. *Eur. J. Inorg. Chem.* **2007**, *2007*, 1473. (b) Pombeiro, A. J. L. *J. Organomet. Chem.* **2005**, *690*, 6021. (c) Zhang, L.; Guedes da Silva, M. F. C.; Kuznetsov, M. L.; Gamasa, M. P.; Gimeno, J.; Frausto da Silva, J. J. R.; Pombeiro, A. J. L. *Organometallics* **2001**, *20*, 2782. (d) Zhang, L.; Gamasa, M. P.; Gimeno, J.; da Silva, M.; Pombeiro, A. J. L.; Graiff, C.; Lanfranchi, M.; Tiripicchio, A. *Eur. J. Inorg. Chem.* **2000**, 1707. (e) Pombeiro, A. J. L. In *Molecular Electrochemistry of Inorganic, Bioinorganic, and Organometallic Compounds*; Pombeiro, A. J. L., McCleverty, J. A., Eds.; Kluwer Academic Publishers: Dordrecht, 1993, p 331.
- (32) van der Eide, E. F.; Piers, W. E.; Parvez, M.; McDonald, R. *Inorg. Chem.* **2007**, *46*, 14.
- (33) Semenov, S. N.; Blacque, O.; Fox, T.; Venkatesan, K.; Berke, H. *J. Am. Chem. Soc.* **2010**, *132*, 3115.
- (34) Semenov, S. N.; Taghipourian, S. F.; Blacque, O.; Fox, T.; Venkatesan, K.; Berke, H. *J. Am. Chem. Soc.* **2010**, *132*, 7584.
- (35) Sun, J.; Shaner, S. E.; Jones, M. K.; O'Hanlon, D. C.; Mugridge, J. S.; Hopkins, M. D. *Inorg. Chem.* **2010**, *49*, 1687.
- (36) Moravec, D. B.; Hopkins, M. D. *Chem.—Eur. J.* **2013**, *19*, 17082.
- (37) The tungsten-containing compounds and their precursors were synthesized using Pd-catalyzed cross-coupling methods similar to those employed in the preparation of organic oligo-phenylene-ethynylenes. The compounds are slightly air sensitive in the solid state and solution. Full details regarding their synthesis and characterization are provided in the Supporting Information.
- (38) Vyboishchikov, S. F.; Frenking, G. *Chem.—Eur. J.* **1998**, *4*, 1439.
- (39) Ofer, D.; Swager, T. M.; Wrighton, M. S. *Chem. Mater.* **1995**, *7*, 418.
- (40) The first reduction potentials of PhCCPh, Ph(CCC₆H₄)₂H, and Ph(CCC₆H₄)₃H in THF have been reported relative to the Ag/Ag⁺ reference as -2.56 V, -2.30 V, and -2.07 V, respectively. Wiberg, J.; Guo, L.; Pettersson, K.; Nilsson, D.; Ljungdahl, T.; Mårtensson, J.; Albinsson, B. *J. Am. Chem. Soc.* **2006**, *129*, 155. These were scaled to the FeCp₂^{0/+}-referenced potentials noted in the text by applying an offset of -0.39 V, which is derived from the reported first reduction potential of PhCCPh in THF against this standard (-2.95 V vs FeCp₂^{0/+}). Boudon, C.; Gisselbrecht, J. P.; Gross, M.; Anthony, J.; Boldi, A. M.; Faust, R.; Lange, T.; Philp, D.; Van Loon, J. D.; Diederich, F. *J. Electroanal. Chem.* **1995**, *394*, 187.
- (41) Chu, Q.; Pang, Y. *Spectrochim. Acta, A* **2004**, *60*, 1459.
- (42) Mao, G.; Orita, A.; Matsuo, D.; Hirate, T.; Iwanaga, T.; Toyota, S.; Otera, J. *Tetrahedron Lett.* **2009**, *50*, 2860.
- (43) Meier, H.; Stalmach, U.; Kolshorn, H. *Acta Polym.* **1997**, *48*, 379.
- (44) Fitting the ³[d_{xy}←π*(WCR)] emission band maxima to eq 1 predicts that for the infinite-length oligomer E_∞ = 12230 cm⁻¹ (818 nm; see Figure 5); this is only 2 nm (20 cm⁻¹) lower than the emission maximum of 4. Thus, the ¹[d_{xy}→π*(WCR)], ¹[π(WCR)→π*(WCR)], and ³[d_{xy}←π*(WCR)] bands all provide effective conjugation lengths of 4–5 units.

(45) Varsányi, G. *Vibrational Spectroscopy of Benzene Derivatives*; Academic Press: New York, 1969.

(46) Schumm, J. S.; Pearson, D. L.; Tour, J. M. *Angew. Chem., Int. Ed.* **1994**, *33*, 1360.

(47) Ishida, H.; Tobita, S.; Hasegawa, Y.; Katoh, R.; Nozaki, K. *Coord. Chem. Rev.* **2010**, *254*, 2449.

(48) Duvanel, G.; Grilj, J.; Schuwey, A.; Gossauer, A.; Vauthey, E. *Photochem. Photobiol. Sci.* **2007**, *6*, 956.

(49) Englman, R.; Jortner, J. *Mol. Phys.* **1970**, *18*, 145.

(50) It was not possible to calculate extinction coefficients for **3** and **4** because their excited-state lifetimes were too close to the temporal response limit of the spectrometer.

(51) Beeby, A.; Findlay, K. S.; Low, P. J.; Marder, T. B.; Matousek, P.; Parker, A. W.; Rutter, S. R.; Towrie, M. *Chem. Commun.* **2003**, 2406.

(52) Sluch, M. I.; Godt, A.; Bunz, U. H. F.; Berg, M. A. *J. Am. Chem. Soc.* **2001**, *123*, 6447.

(53) Levitus, M.; Schmieder, K.; Ricks, H.; Shimizu, K. D.; Bunz, U. H. F.; Garcia-Garibay, M. A. *J. Am. Chem. Soc.* **2001**, *123*, 4259.

(54) Defining the C_{ipso} carbon atom of the phenyl group as C(1), $\delta r = 1/4[r(C(1)-C(2)) + r(C(3)-C(4)) + r(C(4)-C(5)) + r(C(6)-C(1)) - 2r(C(2)-C(3)) - 2r(C(5)-C(6))]$.

(55) Pugliesi, I.; Tonge, N. M.; Hornsby, K. E.; Cockett, M. C. R.; Watkins, M. J. *Phys. Chem. Chem. Phys.* **2007**, *9*, 5436.